Nanoscale Advances

ROYAL SOCIETY OF CHEMISTRY

PAPER

View Article Online
View Journal | View Issue

Cite this: *Nanoscale Adv.*, 2025, **7**, 5536

Stretchable heat-dissipation sheet based on insulating graphene and boron nitride composites: asymmetric elastomeric networks for stable thermal conductivity under repeated tensile strain†

Sang-Mi Jeong, Taekyung Lim, Jonguk Yang, Hee Sung Seo* and Sanghyun Ju *

As modern electronic devices become smaller and more highly integrated, stable thermal management is emerging as a key development approach, including in applications considering mechanical deformation. In this study, a flexible heat-dissipating sheet was developed using composites of insulating graphene (I-Gr), plate-like boron nitride (BN-P), and aggregated spherical BN (BN-A) based on a high-elasticity styrene–(ethylene–butylene)–styrene (SEBS) elastomer. The unique asymmetric two-dimensional layered structure of I-Gr and BN improved the heat transfer properties of the composite by maintaining the continuity of the heat-conducting network despite tensile deformation. In addition, the spherical shape and disordered structure of the aggregated BN-A promoted the formation of an extended heat-conducting path and enhanced the bonding between the fillers. At the optimal composition, the composite maintained an initial thermal conductivity (TC) of 2.0 W m^{-1} K^{-1} or higher, and the TC reduction (ΔTC) was less than 8% and 10% at 50% and 100% elongation, respectively, demonstrating excellent TC stability. In addition, owing to the interfacial affinity and network reinforcing effect of I-Gr, the TC performance and structural stability were maintained even after 500 cycles of 50% tensile strain and 400% elongation. In contrast, the CNT-based composite showed limitations such as low initial TC, large ΔTC, and low elongation. This study presents a design strategy for a heat-dissipating material with high elasticity, high TC, and excellent durability, offering considerable potential for use in next-generation flexible electronic devices such as wearable electronics, freeform displays, and soft robotics.

Received 17th April 2025
Accepted 23rd July 2025

DOI: 10.1039/d5na00373c

rsc.li/nanoscale-advances

Introduction

In modern times, the development of electronic devices and semiconductor technology has been advancing toward high-performance integration. This development, along with the increasing density of electronic devices, further highlights the importance of thermal management.[1] In particular, efficient heat dissipation is essential for applications such as high-power LEDs,[2] semiconductor devices,[3,4] 5G communication equipment,[5,6] electric vehicles, and their battery systems.[7–9] If effective thermal management is not achieved, excessive heat accumulation can lead to performance degradation, reduced reliability, and, in severe cases, physical damage to electronic devices.[10] Traditional heat-conducting substrates provide excellent thermal conductivity (TC); however, they are limited in meeting the demands of modern industries, which require increasingly smaller and more flexible electronic devices. In particular, fixed-shape substrates may not be suitable for flexible or deformable device structures. To address this issue, stretchable heat-conducting substrates have been developed.[11] As the possibilities for freeform displays without shape constraints expand, material innovation with appropriate deformation characteristics and the ability to respond without structural resistance is considered the ultimate goal.

Research on stretchable heat-dissipating substrates has primarily focused on combining thermally conductive fillers with high-elongation elastomers. Stretchable heat-dissipating substrates composed of silicone-based elastomers and liquid metals tend to have increased TC with elongation because of liquid metal deformation during the stretching process forming a heat transfer network.[12,13] However, liquid metals are inherently unstable, and struggle to form heat-transfer networks owing to interparticle repulsion and surface oxidation. In addition, their overall TC is low because they are wrapped in

Major in Nano·Semiconductor, School of Electronic Engineering, Kyonggi University, Suwon, Gyeonggi-do 16227, Republic of Korea. E-mail: hsseo@kgu.ac.kr; shju@kgu.ac.kr

† Electronic supplementary information (ESI) available: The supplementary video is intended to help understand the behavior of the 50% stretching continuous repetition 500 times test for the heat-dissipation sheet based on the I-Gr–BN P/A composite structure manufactured in this study. It shows that the elasticity and mechanical stability are maintained even after hundreds of repeated tensile-recovery deformations. It proves the durability of the high-elasticity network by applying the asymmetric crystal structure filler. See DOI: https://doi.org/10.1039/d5na00373c

elastomers with insulating properties. Additionally, liquid metals are heavy and present significant handling and durability issues, such as the formation of metal oxide layers, leakage risk, and process complexity. In contrast, elastomers based on rigid fillers can efficiently maintain thermal conductivity under deformation even with a relatively small filler content through appropriate filler design, interfacial control, and network structures. They also offer advantages in mechanical durability and ease of commercialization, making them still beneficial stretchable thermal interface materials. However, most existing rigid filler systems face issues such as the collapse of the thermal conduction network under stretching, mechanical damage due to stress concentration, and performance degradation from interfacial debonding. To improve thermal performance, high filler content is often applied, but at high loading, stretchability and elasticity are compromised, resulting in a trade-off between enhanced thermal conductivity and mechanical compliance.[14] For example, a high-content, high-heat-dissipation composite material can be produced by adding hexagonal BN (*h*-BN) to soft polyurethane polymers.[15] In this case, with 50 wt% *h*-BN content, 10.3 W m^{-1} K^{-1} was achieved, and the initial value was maintained after 100 cycles of bending and twisting. However, under 100% elongation, the thermal conductivity decreased to 3.3 W m^{-1} K^{-1}, representing a 68% reduction.[15] When silver nanoparticles were used, thermal conductivity decreased by about 50% under only 25% elongation.[16]

Flexible freeform displays and electronic device applications require focus on ensuring reliability through strategies that maintain robustness under various shape deformations while managing thermal and mechanical stresses. In this study, we fabricated a stretchable heat-dissipating substrate that overcomes the limitations of existing heat-dissipating films by utilizing graphene and BN,[17,18] which are well-known thermally conductive fillers, based on styrene–(ethylene–butylene)–styrene (SEBS), an elastomer with excellent elasticity. In particular, by introducing asymmetric-structured insulating graphene (I-Gr), we formed an anisotropic thermal conduction network, which, due to its asymmetric structure, can rotate and rearrange (sliding/rotation) under stretching without fracturing, helping to maintain thermal pathways and minimize thermal conductivity degradation under deformation compared to conventional rigid fillers. Furthermore, electrical insulation was imparted to ensure device safety. BN, a 2D filler with high thermal conductivity and electrical insulation, contributes to interfacial adhesion through π–π interactions and van der Waals forces with SEBS, helping to distribute loads applied during deformation. Through the combined use of I-Gr and BN and optimal design, we aimed to maintain the filler network during tensile deformation, controlling the stability of the thermal conduction network and the efficiency of stress transfer. By compounding these fillers with SEBS elastomer, we utilized the excellent stretchability and recoverability of SEBS to maintain structural stability under repeated mechanical loading. Through the hybridization of asymmetric graphene and BN in SEBS, we produced a stretchable thermal interface material that simultaneously achieves thermal conductivity, stretchability, and electrical insulation.

Experimental

Material preparation

I-Gr (XCM Inc.; particle size d_{50} 3–5 μm, thickness 300–500 nm, specific surface area <20 m^2 g^{-1}, oxygen content 10–15%), BN-P (CFP006, 3 M; particle size d_{50} 5–8 μm, specific surface area <20 m^2 g^{-1}), BN-A (CFA250S, 3 M; particle size d_{50} 40–100 μm, specific surface area <4.5 m^2 g^{-1}), carbon nanotubes (CNT, MR99, Carbon Nano-material Technology Co., Ltd; particle size d_{50} 5–15 nm, length ∼10 nm, aspect ratio >500, specific surface area 100–700 m^2 g^{-1}) were used as fillers to improve TC. The linear triblock copolymer SEBS (G1645 VO, KRATON Corp., polystyrene content of 11.5–13.5%), was used to form a matrix for the composite while imparting elasticity. Cyclopentyl methyl ether (CPME; ≥99.90%, Sigma-Aldrich) was used as a solvent without further purification.

Fabrication of stretchable heat-dissipation sheets

To uniformly mix I-Gr into the SEBS matrix, UV-ozone treatment was performed on both sides for 30 min each for a total of 1 h using a UVO Cleaner (AH-1700, AhTECH Leading Technology Systems Co., Korea) to remove surface organic substances and modify the surface. The surface-treated graphene (I-Gr) was added to 1.0 wt% CPME solvent and dispersed for 1 h using a sonicator (SD-D400H, Sungdong Ultrasonic Co., Korea). To prevent overheating and oxidation, the ultrasonic device was set to a frequency of 40 kHz and power setting of 40% for 15 min each for four cycles. SEBS was added to the dispersed solution at 20 wt% relative to CPME and mixed using a paste mixer (HGT-4000DI, LM TECH., Korea) at 800 rpm for 5 min each for four cycles. BN-P and BN-A were then added to this solution in a 1 : 2 ratio such that the BN-P/A composite component was 14 wt% relative to CPME. Mixing was performed with a paste mixer for 5 min. The mixed I-Gr–BN-P/A–SEBS mixture was cast onto a glass substrate to a thickness of 1 mm and air dried at room temperature (∼25 °C) for more than 30 min. Subsequently, it was dried in a forced-convection oven (LO-FS100, LK LAB KOREA lnc.) at 90 °C for over 12 h to completely remove residual solvents. The dried I-Gr–BN-P/A–SEBS sheet was heat-compressed at 170 °C and 400 kg cm^{-2} using a hot press (QM900L, QMESYS, Korea), minimizing heat damage by limiting hot-press contact to 5 min. The resulting I-Gr–BN-P/A–SEBS-based stretchable heat-dissipation sheets had constant thicknesses of 0.35 mm.

Characterization of stretchable heat-dissipation sheets

The fabricated I-Gr–BN-P/A–SEBS-based stretchable heat-dissipation sheet was cut to a size of 60 × 80 mm. The in-plane TC was measured using a Hot Disk (TPS 2500S, Hot Disk®, Sweden) to evaluate the thermal properties without physical deformation. A TC sensor (5465 F2, Kapton-insulated Sensors) with an effective measurement area of 3.2 mm diameter was used. The specimen was attached above and below the

sensor and pressed with a weight to flatten it. The measurements were performed thrice for 10 s each in the in-plane direction at a heating power of 20 mW, and the average value was calculated. To evaluate the thermal properties of the stretchable heat-dissipation sheets according to their elongation, a horizontal cyclic elongator (COAD 526, Ocean Science Co., Korea) was used to continuously apply repeated elongation deformation. The specimen was stretched to the maximum elongation achievable without damage or breakage, and the elongation (%) relative to the initial length was calculated. A Hot-Disk sensor was installed in the cyclic elongator to measure TC in the elongated state (stationary) and the variation in TC under cyclic elongation. The retention of TC properties before and after stretching was quantified using the TC change rate calculation formula, $\Delta TC\ (\%) = (TC_{0\%} - TC_{50\%})/TC_{0\%} \times 100$ ($TC_{0\%}$: measured initial TC, $TC_{50\%}$: measured TC at 50% tensile strain).

The alignment and morphological changes of the fillers due to stretching were observed by examining the cross-section using scanning electron microscopy (SEM; JSM-7401F, JEOL, Japan). The heat dissipation performance was assessed by visualizing the heat generation and distribution patterns of the area where the sheet was applied using an infrared camera (T420, FLIR® Systems, Inc., Oregon, USA). Furthermore, a stretchable heat-dissipation sheet was placed on top of a hot plate set to 50 °C and the temperature was continuously measured over a set amount of time at room temperature (25 °C).

The mechanical property of the heat-dissipation sheet was measured using a universal testing machine (UTM, Lloyd Instruments, Ametek LD10). Under ambient conditions, a uniaxial tensile load of 100 N was applied, and tensile testing was performed at a constant speed of 100 mm min^{-1} until fracture occurred, while collecting stress–strain data. The tensile specimens were fixed at a thickness of 350 μm and cut into a dog-bone shape (width 10 mm, gauge length 25 mm) so that fracture would occur in the central region of the specimen, by ASTM D882 (standard test method for tensile properties of thin plastic sheets, less than 1.0 mm in thickness) (using QMESYS, Q-14).

Results and discussion

Fig. 1(a) illustrates a schematic diagram of the flexible heat-dissipating sheet developed in this study. Using SEBS elastomer as a matrix to form composites with I-Gr, BN-P, and BN-A, a flexible heat management material was fabricated. The composite was designed to support the formation of a thermal conduction path despite having a complex shape or being subjected to mechanical stress while exhibiting flexibility and elasticity that allow surface attachment. Graphene and BN have standard two-dimensional (2D) van der Waals layered structures and exhibit excellent heat transfer properties owing to the anisotropy of their in-plane and inter-plane thermal conductivities.[19–21] In particular, the I-Gr used in this study is a partially exfoliated form of graphene, which introduces asymmetric structural defects into the hexagonal lattice.[22] This configuration effectively provides electrical insulation and TC by lowering the electrical conductivity and strengthening interlayer interactions. Traditional graphene has high TC (~5300 W m^{-1} K^{-1}), low density (2.2 g cm^{-3}), and excellent flexibility, making it promising as a thermally conductive material; however, its high electrical conductivity limits its application in highly integrated electronic devices.[22,23] I-Gr addresses these issues and help maintain the stability of the heat-conducting network even under tensile conditions through its structural asymmetry. Meanwhile, BN is also based on a hexagonal crystal structure and has an asymmetric 2D arrangement of alternating nitrogen and boron atoms. This structural characteristic enhances the anisotropy of the phonon dispersion and induces the formation of zigzag-shaped heat transfer paths, contributing to accelerated heat diffusion.[19,24] Because *h*-BN has a lattice structure similar to that of I-Gr, a stretchable and thermally conductive heterostructure was designed by mixing them, allowing effective retention of the geometrical thermal properties of I-Gr. This study attempted to further increase the efficiency of heat conduction along the in-plane direction by utilizing the asymmetry of the I-Gr and *h*-BN crystal structures. In addition, the layered structure bonded by weak van der Waals forces has soft lubricating properties; therefore, it can effectively exhibit stretchability. Based on these characteristics, BN-P and BN-A were mixed and applied together with I-Gr to design a thermal conduction path that could be stably maintained under deformation. In particular, we evaluated whether the structural disorder and agglomeration of BN-A can positively promote thermal conductivity.

Fig. 1(b) shows a schematic of the actual manufacturing process of a flexible heat-dissipating sheet. Layered plate fillers were aligned in the plane direction through heat pressing, thereby effectively forming an in-plane heat conduction path and implementing a heat-dissipation sheet with a high-elasticity network. Fig. 1(c) exhibits the tensile properties of the fabricated I-Gr–BN-P/A–SEBS composite sheets. The specimen has excellent elongation of up to 400% using manually applied force. Fig. 1(d) shows the results of evaluating the heat dissipation performance by placing the sheet on a 50 °C hot plate while maintaining a 400% tensile strain. When comparing the I-Gr–BN composite sheet with an unmodified SEBS sheet under identical conditions, the composite sheet exhibited faster heat dissipation and a slower increase of surface temperature. The maximum surface temperature after 180 s was 45.4 °C, approximately 5 °C lower than that of the unmodified SEBS sheet (50.8 °C), indicating that the thermally conductive network of the composite was effectively maintained even in a high-elongation state and that excellent heat dissipation performance was sustained. As a result, the I-Gr–BN-P/A composite, composed of asymmetrically structured insulating graphene and BN fillers of various shapes, simultaneously exhibited 2D thermal conductivity characteristics and excellent elasticity, demonstrating a heat-dissipation sheet with stable thermal conductivity performance under mechanical deformation.

The TC and ΔTC under static and tensile conditions were analyzed by introducing composites of one-dimensional (1D)

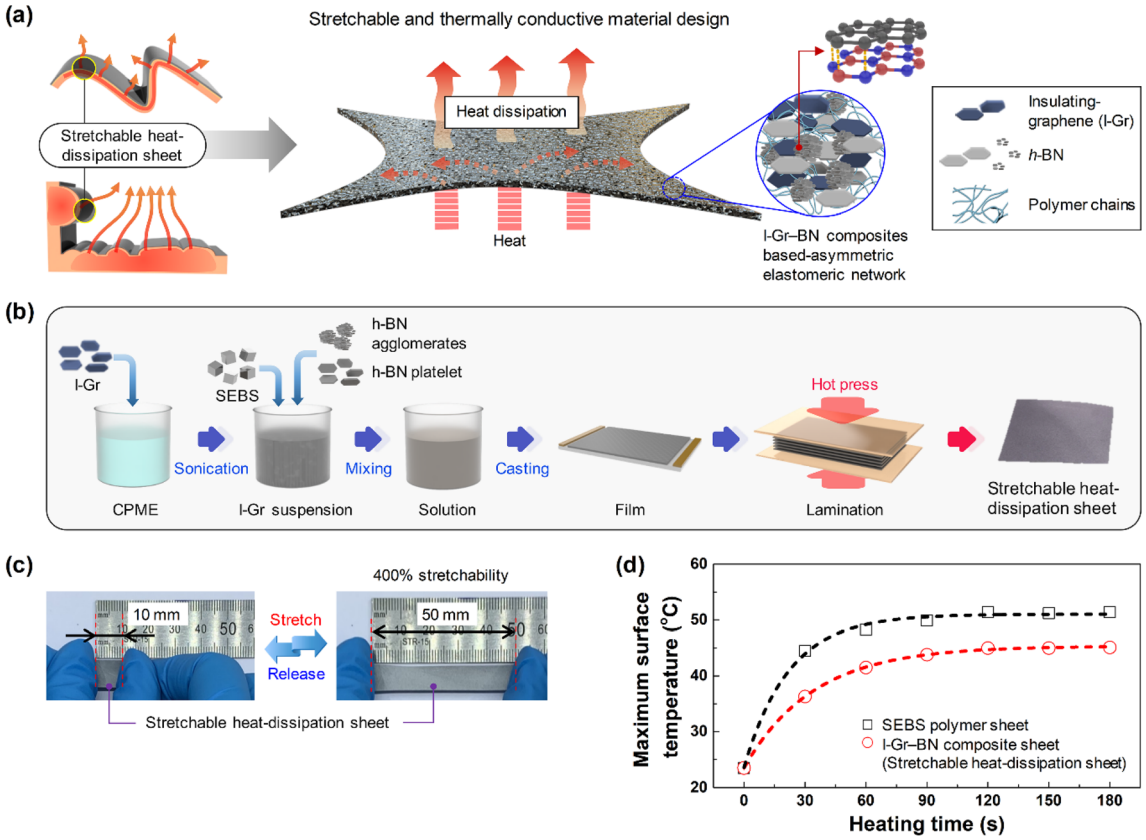

Fig. 1 Concept, fabrication process, and heat dissipation performance evaluation of I-Gr–BN-based stretchable heat-dissipation sheets. (a) Schematic diagram of the thermally conductive network composed of insulating graphene (I-Gr) and heterogeneous BN fillers (BN-P, BN-A) in the SEBS polymer matrix. (b) Schematic diagram of the fabrication process of the I-Gr–BN composite stretchable heat-dissipation sheet. (c) Mechanical elongation performance of the composite sheet. (d) Comparison of heat-dissipation performance under 400% tensile strain.

and 2D thermally conductive fillers (1D CNT, 2D I-Gr, and 2D BN-P) into the SEBS-based polymer matrix. In particular, the formation pattern of the composite filler networks and the difference in heat transfer performance were compared with respect to the filler-to-filler interaction owing to the structural characteristics of the fillers (1D *vs.* 2D) and the interfacial compatibility with SEBS. The TC and ΔTC under tension of each composite were compared based on the 50% tension condition. The $TC_{0\%}$ and $TC_{50\%}$ were measured immediately after fabrication (TC 1st) and measured a second time after an aging step (TC 2nd), in which the material was left at room temperature for 40 min in an elongated state.

Fig. 2(a) shows a schematic diagram of the in-plane thermal conductivity measurement by the Hot Disk instrument. Fig. 2(b) shows $TC_{0\%}$, $TC_{50\%}$, and ΔTC for composites in which the I-Gr content was increased from 0 to 20 wt% while maintaining BN-P content at 70 wt%. As the I-Gr content increased, the thermal conductivity also increased. At 20 wt%, the initial thermal conductivity showed a remarkable improvement of approximately 2.75 W m^{-1} K^{-1} because the 2D planar structure of graphene can efficiently form a heat-transfer path. Exfoliated asymmetric I-Gr effectively alleviated the interfacial resistance between BN and SEBS. In particular, the composite with 10 wt% graphene exhibited a minimum ΔTC of 13% after aging, indicating improved thermal conductivity stability under tensile strain, attributed to the synergistic effect between I-Gr and BN, as well as the improved interfacial compatibility due to I-Gr. Additionally, the 2D interlayer thermal network that is extended and rearranged through the aging process appears to be optimal for correcting the strain within the matrix and for sufficient dispersion to activate and stabilize phonon transport.

Fig. 2(c) shows the TC characteristics when the BN-P content was varied from 50 to 90 wt%, while the graphene content was maintained at 10 wt%. As the BN content increased, the $TC_{0\%}$ increased, with a particularly high value of approximately 3.0 W m^{-1} K^{-1} at 90 wt% BN-P. However, the increase in BN content caused an undesirable gradual increase in the ΔTC, with a value approaching 30% at 90 wt% BN-P, due to tension. Excessive addition of BN-P exceeding 70 wt% significantly increased ΔTC, indicating that increased BN-P addition is unfavorable for the application. When the concentration of BN-P, possessing a 2D plate-like structure, was increased while maintaining 10 wt% I-Gr, which also has a 2D structure, the initial interaction between similar asymmetric crystal layers was improved. However, when tensile strain was applied, a gap appeared between the layered fillers, which were in parallel contact, shortening the travel distance of phonons, which ultimately reduced the thermal conductivity significantly. The increasing

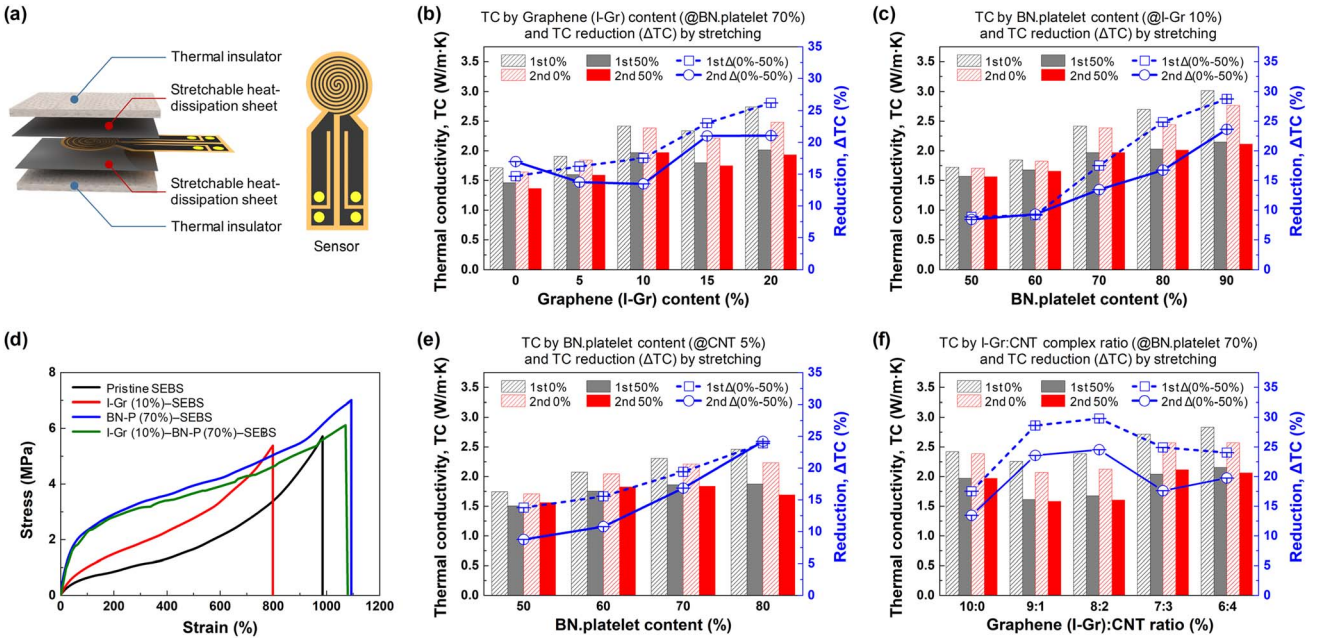

Fig. 2 Thermal conductivity (TC) and tensile thermal conductivity reduction (ΔTC) analysis results for SEBS-based composites with one- and two-dimensional fillers. (a) Schematic diagram of the in-plane thermal conductivity measurement. (b) TC and ΔTC with varying insulating-graphene (I-Gr) content (0–20 wt%) and a fixed 70 wt% BN platelet (BN-P) content. (c) TC and ΔTC with increasing BN-P content (50–90 wt%) and fixed 10 wt% I-Gr. (d) Strain–stress curves of pristine SEBS, I-Gr (10%)–SEBS, BN-P (70%)–SEBS, and I-Gr (10%)–BN-P (70%)–SEBS sheets. (e) TC and ΔTC with increasing BN-P content and fixed 5 wt% carbon nanotubes (CNT). (f) TC and ΔTC with varying I-Gr : CNT ratios (10 : 0–6 : 4; 10 wt% in total) and fixed 70 wt% BN-P. 1st: Immediate TC measurements after fabrication. 2nd: TC measurements after leaving the sample in an elongated state in room temperature for 40 min.

trend of ΔTC with increasing BN gradually decreased to 23% in the second measurement, indicating that mutual van der Waals bonds were formed between the I-Gr–BN crystal layers rearranged by the initial stretching and subsequent aging processes.

As shown in Fig. 2(d), when the matrix consisted of SEBS alone, the tensile strength was 6.28 MPa and the strain at break was 980%. When I-Gr was added alone (I-Gr–SEBS), the tensile strength decreased to 5.4 MPa and the strain at break to 800%, indicating reduced tensile properties. In contrast, when BN-P (70 wt%) was added (BN-P–SEBS), the tensile strength and strain at break increased to 7.0 MPa and 1100%, showing excellent deformation characteristics. This suggests that BN in the SEBS matrix favorably contributes to improving the deformation limit characteristics at the fracture point, while I-Gr tends to attenuate such deformation properties.

As a result, the tensile properties of the I-Gr–BN-P–SEBS heat-dissipation sheet (tensile strength 6.2 MPa, strain at break 1120%) showed that the enhancing effect of BN strongly compensated for the degradation effect of I-Gr, demonstrating the complementarity of the reinforcement mechanisms between the fillers. This indicates that the combined structure of the two fillers effectively manifested the load-bearing role of I-Gr (enhancing interfacial stress) and the load transfer-dispersion role of BN-P (improving elongation properties) through their excellent mutual interactions. BN-P disrupted the strong π–π stacking between I-Gr layers and suppressed aggregation, thereby increasing interfacial contact between I-Gr and SEBS and forming van der Waals bonding between I-Gr and BN-P.

BN-P was not involved in I-Gr layers, nor was it bound *via* van der Waals interactions to I-Gr; however, it directly interacted with SEBS, leading to increased interfacial bonding and improved load sharing, which resulted in better elongation. In this process, the styrene blocks in SEBS formed π–π interactions with I-Gr, and van der Waals and partial π–π-like interactions with BN-P, creating multiple interfacial bonds through different interaction pathways within the composite. Consequently, stress transfer paths diversified, stress concentration was dispersed, and interfacial mobility increased, allowing the filler network to be maintained and adapt flexibly under deformation conditions.

In other words, by combining I-Gr and BN-P with similar asymmetric 2D crystal structures, the van der Waals forces acting between them were optimized for molecular and interfacial bonding within the SEBS polymer matrix, enabling the stable realization of a van der Waals heterostructure with excellent tensile properties.

Fig. 2(e) shows the result of introducing 1D CNT instead of 2D graphene. The introduction of CNT was expected to compensate the decrease in TC by forming a linear phonon path in the thermally empty space owing to the separation between the layered fillers due to tensile strain. In the composite where 5 wt% CNT was introduced, the BN-P content was varied from 50 to 80 wt%. When >5 wt% CNT was introduced, elasticity diminished, and the sheet fractured at 50% elongation. While

graphene enabled the production of elastic sheets when concentrations were within 10 wt%, CNTs negatively affected the elastic properties across all tested compositions. For the composite with 5 wt% CNTs, the $TC_{0\%}$ was relatively low overall, and even when the BN content reached 80 wt%, the $TC_{50\%}$ 2nd was limited to 1.69 W m^{-1} K^{-1}, attributed to the 1D fiber-like structure of CNTs; therefore, the contact surface between the fillers is limited. The network connectivity between the particles did not increase sufficiently during elongation and so heat transfer paths were not efficiently formed. As the BN-P content increased, the ΔTC under tension significantly increased more compared to that of the graphene-based composition, likely due to the introduction of CNTs limiting the properties of BN and causing local vulnerabilities in alleviating the interfacial thermal resistance between BN and SEBS and the bonding structure between BN layers. This observation is also evident in the increasing trend of TC reduction observed in the secondary measurements after aging. In addition, for this composition, the mechanical elongation limit was limited to less than 200%, and the TC during tension tended to decrease rapidly to more than 25%, attributed to the structural limitations of the CNT-based composites and the existence of interfacial resistance.

Fig. 2(f) compares the TC and ΔTC while varying the I-Gr : CNT ratio (fixed to 10 wt% total carbon filler and 70 wt% BN-P). When an I-Gr : CNT of 8 : 2 or 9 : 1 was used, ΔTC significantly increased to approximately 25% compared to that of I-Gr alone (10 : 0), which exhibited a 13% decrease, thus confirming that the I-Gr-based composite design was superior to that utilizing CNT in terms of maintaining the thermal conductivity under tensile conditions because the 2D I-Gr network overcame the 1D structural limitations of CNT and stabilized the heat-transfer path. However, compared to the composite based on I-Gr alone, the initial TC of the 1D–2D carbon composite structure was generally higher. ΔTC tended to increase and showed limitations in mechanical extensional deformation, therefore optimization of the composition design between fillers was required.

Fig. 3(a) shows the thermal conductivity behavior of graphene composite sheets based on the ratio of BN-A and BN-P. From the experimental results in Fig. 2, the composition of 10 wt% I-Gr and 70 wt% total BN was derived as the condition for the maximum elongation change% and the minimum ΔTC under tension. When the BN platelet : agglomerates (BN P : A) ratio was 1 : 2, the $TC_{0\%}$ measured was 2 W m^{-1} K^{-1}. After aging, the ΔTC was maintained at less than 10% (approximately 8.2%) even in the tensile state (based on 50% elongation), thus satisfying the general reliability criterion of ΔTC < 10%—typically used for electronic devices. This result is believed to be because the spherically aggregated BN-A particles maintain fluidity and flexibility characteristics within the matrix, thereby improving their dispersibility and fluidity by forming a three-dimensional (3D) multicontact connection structure between the 2D layered structures of I-Gr and BN. The expanded contact area enabled stable thermal contact, and the network collapse between fillers due to elongation was suppressed. In addition, recent studies have reported that the surface roughness, microscopic cavities, and pore structures of filler particles play important roles in the formation of heat transfer paths within polymers.[19,20] During the composite sheet manufacturing process, the microscopic cavities formed by the polymer fluid at the particle surface and interface can act as nucleation sites for heat propagation, and the structural disorder and surface characteristics of agglomerated BN-A contribute to maintaining the thermal conductivity through a complex action.

Fig. 3(b) shows the changes in TC and ΔTC according to the variation in thickness (300–500 μm) using the previously optimized composite filler composition of I-Gr–BN-P/A (P : A of 1 : 2). As the thickness decreased, the $TC_{0\%}$ increased, whereas the ΔTC during tension gradually decreased. In particular, ΔTC showed a minimum value of less than 10% (approximately 8.2%) when the composite thickness was 350 μm because the asymmetric interlayer van der Waals bonds of the thermally conductive filler became more firmly connected and stably maintained as the thickness decreased. The structural collapse of the filler was suppressed even under tensile deformation, thereby alleviating the loss of TC due to elongation. On the other hand, the reason why the TC increases along with the decrease in thermal conductivity during elongation at a thickness of 300 μm is that some of the interlayer bonding tissue of the crystal may be damaged during the manufacturing process at a low thickness, causing local deformation and a decrease in thermal conductivity in response to elongation stress.

In Fig. 3(c), the changes in TC and ΔTC were measured after continuous cyclic application of 50% elongation for 500 cycles. Even after hundreds of these elongation cycles, the measured TC was maintained without a significant decrease compared to the initial value, and ΔTC was also stably maintained below 10%, indicating that the filler network within the composite provided structural stability even under repeated mechanical stress. In addition, the TC recovery upon returning to the initial length was excellent, indicating that the elastic network of the composite contributed to both resilience and thermal stability. (Refer to the ESI† to understand the behavior of the 50% stretching continuous repetition 500 times).

Fig. 3(d) shows the durability of the thermally elastic network at higher levels of elongation (400%). Repeated tests were performed up to 20 times to determine whether the initial thermal conductivity could be maintained after elongation to 400% and reversion to the original length; the changes in TC and ΔTC before and after elongation were measured. The results indicate that the TC (2.08 W m^{-1} K^{-1}) in the state where the thermal network was stabilized through aging and the TC (2.03 W m^{-1} K^{-1}) in the state where the stress-induced change was experienced through high elongation were nearly recovered to the initial values, and that the ΔTC of the sheets before and after elongation were maintained below 5% throughout the 20 cycles, implying that the asymmetric 2D and 3D networks between the composite fillers were effectively maintained even under high elongation conditions and that the interfacial bonding strength reinforced by I-Gr provided structural toughness that could withstand high elongation stress.

Fig. 4(a) shows the strain–stress curve of the I-Gr–BN P/A–SEBS composite heat-dissipation sheet. It exhibits the typical S-shaped trend of an elastomer and demonstrates excellent

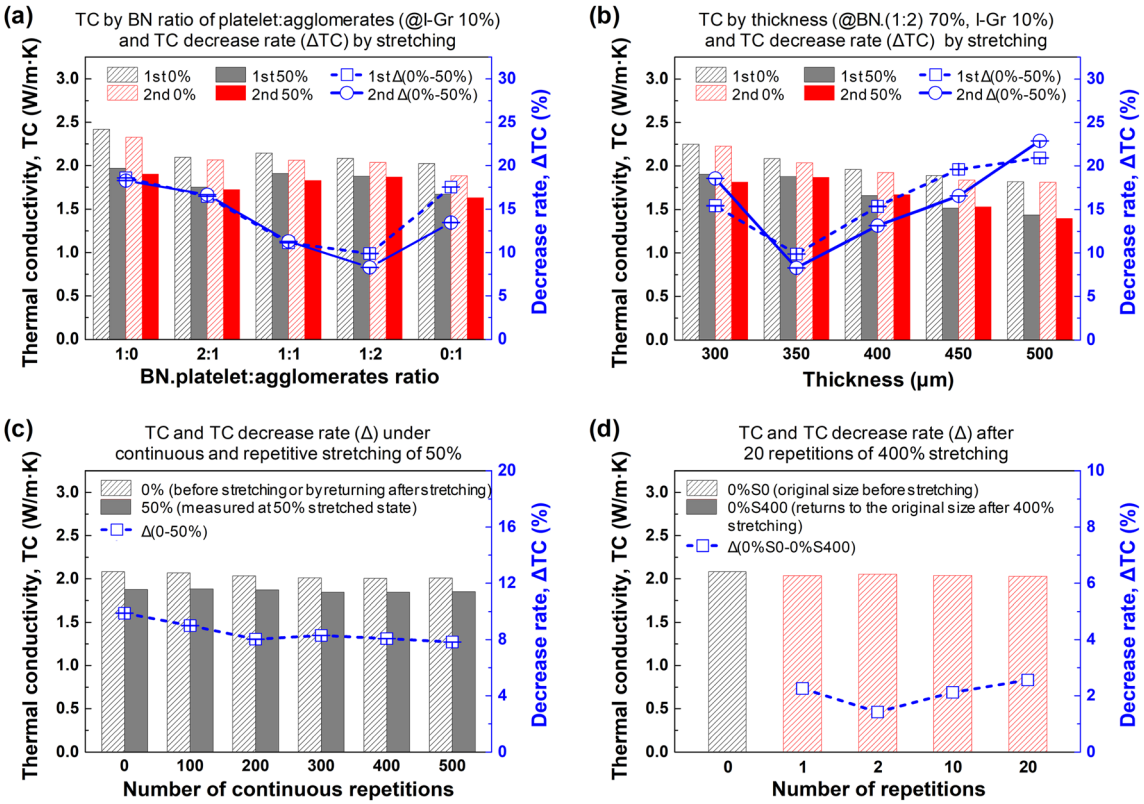

Fig. 3 Thermal conductivity (TC) and thermal conductivity reduction (ΔTC) of the composite sheets according to BN filler geometry, film thickness, and cyclic stretching conditions. (a) TC and ΔTC as a function of the BN platelet : agglomerates ratio at 10 wt% graphene (I-Gr). (b) TC and ΔTC as a function of composite thickness (300–500 μm). (c) TC and ΔTC after continuous stretching (0–500 cycles) at 50% elongation. (d) TC and ΔTC as a function of cyclic stretching-recovery (0–20 cycles) at a high elongation of 400%.

mechanical deformation properties, with an average tensile strength of 6.6 MPa and a strain at break of 1120%. These outstanding deformation characteristics are attributed to the elastomeric bonding of the SEBS matrix, the interfacial bonding between the matrix and the fillers, and the synergistic effects of the I-Gr and BN-P/A fillers.

Fig. 4(b) shows the results of a stepwise tensile test from 0 to 400% for the composite sheet, indicating that the uniform elongation and shape deformation of the specimens were well maintained. The specimen retained its structural integrity even under high elongation conditions, withstanding tensile forces without fracture or local damage, indicating that the network of fillers in the composite sheet was formed robustly against the mechanical load.

Fig. 4(c) shows the results of measuring the mechanical fatigue properties of the I-Gr–BN-P/A–SEBS composite heat-dissipation sheet under repeated loading, using a UTM. While applying high deformation up to 400% strain, tensile-recovery cycles were repeated 100 times, during which elastic relaxation behavior was observed. In this fatigue test, an aging step was applied to the specimen (initial stretching to 50% strain, then left at room temperature for 40 minutes to recover), inducing the fillers to reorient and rearrange after initial stretching and stabilizing the filler network and interfacial bonding within the matrix so the structure could recover to its original conduction channels.

After aging, the strain–stress curves obtained at each cycle, up to a total of 100 repetitions, were compared. The deformation strength for the first 400% stretch (black line) was 1.5 MPa, and as repeated tensile-recovery deformation progressed, the strength decreased very gradually, with the fatigue strength at the final 100th cycle (purple line) reaching ~1.2 MPa. The reduction in deformation strength after 100 repetitions of 400% strain in the SEBS matrix composite system with asymmetric graphene I-Gr and *h*-BN fillers is reasonably attributed to microdamage caused by repeated loading. SEBS, as a thermoplastic elastomer, withstands high-strain deformation well, but can be sensitive to fatigue from repeated deformation. During repetition, the chain alignment–relaxation–realignment process occurs continuously, and in this process, slip between molecular chains and internal friction can accumulate, leading to a gradual decline in strength.

While I-Gr and BN fillers generally impart mechanical strength and thermal conductivity to SEBS, under repeated loading, they can become stress concentration points and potential initiation sites for microcracks.[25] In particular, BN may have weaker interfacial bonding than graphene, which has strong π–π interactions, making damage initiation more likely around BN. Therefore, in polymer material systems where fully elastic recovery is difficult under high-strain repetition, such gradual decreases in deformation strength are often interpreted

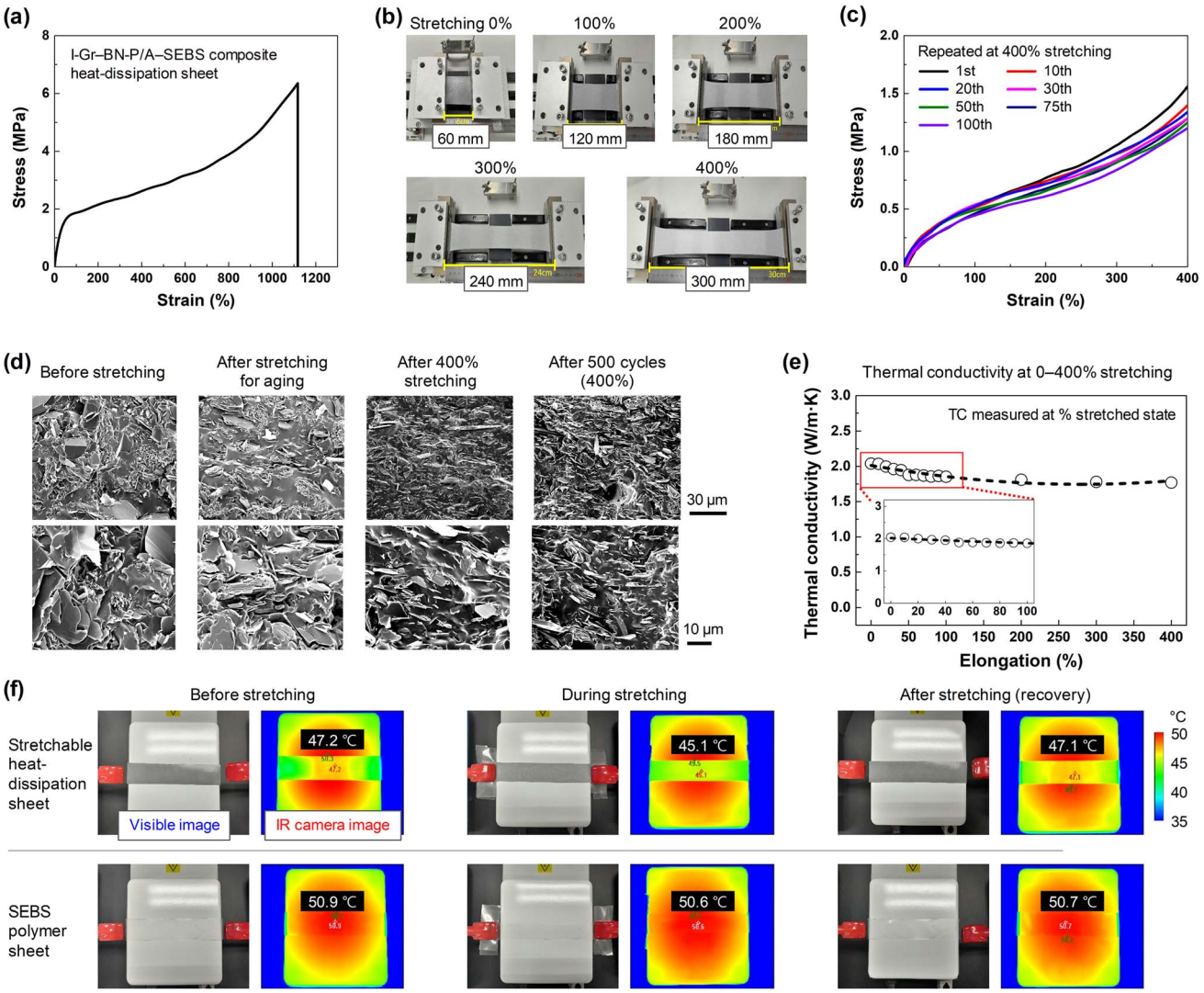

Fig. 4 Evaluation of mechanical properties, structural stability, and heat dissipation performance of I-Gr–BN-P/A–SEBS composite sheets under varying elongation conditions. (a) Strain–stress curve of I-Gr–BN-P/A–SEBS composite heat-dissipation sheet. (b) Stretching of the specimen at different elongation levels of 0–400%. (c) Strain–stress curves of repeated at 400% stretching. (d) Cross-sectional FE-SEM images before elongation, after aging, after 400% elongation, and after 500 cycles of elongation (400%). (e) Thermal conductivity measured at various elongations (0–400%). (f) Infrared thermographic images of I-Gr–BN-P/A-based composite sheets and SEBS sheets.

as evidence of microdamage (microcracks, molecular chain damage, *etc.*).[26–28]

Nevertheless, after each stretching cycle, the strain returned nearly to the original starting position, showing convergence over 100 cycles. Compared to the first stretch, stiffness decreased (softening) upon returning and re-stretching from the second cycle onward. Still, during subsequent repeated stretching, deformation occurred from this reduced stiffness state, indicating that recovery after unloading was maintained. The I-Gr–BN filler network within the aged SEBS matrix was observed to largely recover its original state after repeated deformation, without undergoing further stiffness changes due to polymer chain extension and rearrangement.

Fig. 4(d) shows the cross-sectional FE-SEM observation results of the specimen before and after elongation and under repeated elongation conditions (aging after 50% elongation, 400% elongation, and 500 cycles). Initially, the plate-like I-Gr and the combination of plate-like and spherical BN composite fillers were uniformly dispersed within the SEBS matrix; moreover, the contact structure between the fillers was relatively well maintained even after elongation. High magnification (1 μm) observation results showed that no significant filler disconnection or interface delamination was observed even under repeated elongation conditions (400% elongation × 500 times). The elongation direction orientation and interlayer bonding structure of the filler were improved through repeated elongation processes, indicating that the internal network of the composite was structurally stable even under repeated mechanical stress.

Fig. 4(e) shows the results of directly measuring TC while maintaining the elongation state after deforming the specimen according to various elongations in the range of 0–400%. As the

elongation increased, the TC gradually decreased. At tensile strains of 50% and 100%, the thermal conductivity reduction rate (ΔTC) was less than 8% and 10%, respectively, confirming excellent thermal conductivity stability. Under high tensile strain conditions up to 400%, ΔTC gradually decreased to a maximum of about 13%. Therefore, the practical tensile condition satisfying the ΔTC <10% criterion, generally used as a reliability standard for electronic devices, is considered to be up to 100% strain.

Fig. 4(f) evaluates the temperature distribution of an actual heat-emitting specimen with an infrared thermal imaging camera and compares the temperature distribution changes before and after stretching for the I-Gr–BN-P/A-based composite sheet and an unmodified SEBS sheet. The I-Gr–BN-P/A composite sheet placed on a surface heated to 50 °C maintained a low temperature of 47.2–47.1 °C at the center with minimal change after stretching and recovery, whereas the SEBS pad showed a high temperature of 50.9–50.7 °C at the center. In particular, the I-Gr–BN-P/A composite sheet during elongation exhibited accelerated heat dissipation with a decrease in the center temperature to 45.1 °C. Conversely, the SEBS pad exhibited poor heat dissipation, with a high temperature of 50.6 °C measured even during elongation, indicating that the asymmetric 2D elastic network based on the I-Gr–BN-P/A composite filler maintained an excellent heat diffusion capability even under elongation conditions, suggesting its suitability for applications requiring stable heat dissipation performance under mechanical deformation.

Conclusions

In this study, a stretchable heat-dissipating sheet was developed by combining I-Gr, BN-P, and BN-A based on a SEBS polymer matrix to achieve both mechanical stretchability and excellent thermal conductivity. In particular, the composite composition of I-Gr and BN with an asymmetric two-dimensional van der Waals layered structure maintained a stable network without any break in the heat conduction path even under tensile strain conditions, and the performance was demonstrated to satisfy the thermal conductivity stability criterion (ΔTC <10%) required for electronic device applications.

I-Gr enhanced the interfacial affinity with SEBS, strengthened the bonding force between the fillers and the formation of internal heat transfer paths in the composite, and exhibited strong synergy in the asymmetric layered bonding with BN. The BN-P and BN-A composites formed a three-dimensional (3D) multicontact connection structure between the two-dimensional (2D) layered structures of I-Gr and BN. They effectively suppressed the collapse of the filler network due to deformation by strengthening the structural disorder and particle fluidity. In particular, when the ratio of BN P : A was configured as 1 : 2, an initial thermal conductivity of 2 W m^{-1} K^{-1} or higher was attained, and the thermal conductivity reduction was maintained at 8% and 10% in the 50 and 100% tensile states, respectively, due to the rearrangement of the thermal network and increase in bonding strength between the composite fillers after aging. Despite continuous repetition of 50% tensile stress application up to 500 cycles, the TC decreased no more than 10%. Even after high elongation of up to 400% and tensile recovery, the composite maintained a thermal conductivity performance of 2 W m^{-1} K^{-1} with a minimum thermal conductivity reduction of approximately 5% during 20 cycles. This result implies that the asymmetric 2D layered bonding and 3D elastic network within the composite were structurally stable, even under repeated mechanical loads, and have high resilience. Meanwhile, the CNT-based composite examined as a comparative group attempted to compensate for the decrease in thermal conductivity due to elongation through a one-dimensional (1D) connection path, but the measured initial thermal conductivity was low at 1.6 W m^{-1} K^{-1}, and the thermal conductivity reduction greatly increased by more than 25% when stretched. In addition, its mechanical elongation was also limited to less than 200%, limiting its practical application as an elastic heat-conducting material. This is attributed to the limitations of the linear structural characteristics of CNTs, which restrict heat dissipation only in the longitudinal direction, and the resulting inefficiency in forming an extended heat conduction path within the polymer.

The developed stretchable heat-dissipating sheet based on the I-Gr–BN composite structure fully demonstrated its potential as a highly functional thermally conductive material with the thermal conductivity stability, mechanical flexibility, and structural reliability required for electronic devices. This material is expected to be widely used in various next-generation electronic device applications such as wearable electronic devices, freeform displays, soft robotics, stretchable sensors, and electronic skin.

Data availability

The data that support the findings of this study are available from the corresponding author upon reasonable request.

Conflicts of interest

The authors declare no completing financial interests.

Acknowledgements

This work was supported by the National Research Foundation of Korea (NRF) grant funded by the Korea government (MSIT) (RS-2020-NR049541, RS-2022-NR069927, RS-2024-00357747, RS-2024-00358162, and RS-2025-00561597).

References

1 A. L. Moore and L. Shi, *Mater. Today*, 2014, **17**, 163–174.
2 J. Liu, Y. Mou, Y. Huang, J. Zhao, Y. Peng and M. Chen, *Micromachines*, 2022, **13**, 958.
3 L. Ding, R. Song, S. Zhao, J. Wang and H. A. Mantooth, *IEEE Trans. Power Electron.*, 2023, **38**, 11507–11520.
4 T. Funaki, S. Fukunaga, T. Hara and T. Ibuchi, *2022 International Power Electronics Conference (IPEC-Himeji 2022-ECCE Asia)*, Himeji, Japan, 2022.

5 Y. Song, C. Perez, G. Esteves, J. S. Lundh, C. B. Saltonstall, T. E. Beechem, J. I. Yang, K. Ferri, J. E. Brown, Z. Tang, J.-P. Maria, D. W. Snyder, R. H. Olsson III, B. A. Griffin, S. E. Trolier-McKinstry, B. M. Foley and S. Choi, *ACS Appl. Mater. Interfaces*, 2021, **13**, 19031–19041.
6 C. Tong, in *Advanced Materials and Components for 5G and Beyond*, Springer Nature Switzerland, Cham, 2022, pp. 173–215, DOI: 10.1007/978-3-031-17207-6_7.
7 V. Talele, P. Thorat, Y. P. Gokhale, A. Chandak and V. K. Mathew, in *Energy Storage Systems: Optimization and Applications*, ed. V. K. Mathew, T. K. Hotta, H. M. Ali and S. Sundaram, Springer Nature Singapore, Singapore, 2023, pp. 303–342, DOI: 10.1007/978-981-19-4502-1_15.
8 V. G. Choudhari, D. A. S. Dhoble and T. M. Sathe, *J. Energy Storage*, 2020, **32**, 101729.
9 A. Tikadar, D. Johnston, N. Kumar, Y. Joshi and S. Kumar, *Appl. Therm. Eng.*, 2021, **183**, 116182.
10 C. Zhao, Y. Li, Y. Liu, H. Xie and W. Yu, *Adv. Compos. Hybrid Mater.*, 2022, **6**, 27.
11 N. Matsuhisa, X. Chen, Z. Bao and T. Someya, *Chem. Soc. Rev.*, 2019, **48**, 2946–2966.
12 M. D. Bartlett, N. Kazem, M. J. Powell-Palm, X. Huang, W. Sun, J. A. Malen and C. Majidi, *Proc. Natl. Acad. Sci. U. S. A.*, 2017, **114**, 2143–2148.
13 S. H. Jeong, S. Chen, J. Huo, E. K. Gamstedt, J. Liu, S.-L. Zhang, Z.-B. Zhang, K. Hjort and Z. Wu, *Sci. Rep.*, 2015, **5**, 18257.
14 Z. Yin, J. Guo and X. Jiang, *Compos. Sci. Technol.*, 2021, **209**, 108794.
15 H.-J. Hong, S. M. Kwan, D. S. Lee, S. M. Kim, Y. H. Kim, J. S. Lim, J. Y. Hwang and H. S. Jeong, *Compos. Sci. Technol.*, 2017, **152**, 94–100.
16 A. A. Jan, D. Suh, S. Bae and S. Baik, *Nanoscale*, 2018, **10**, 17799–17806.
17 W. Ye, Z. Ye, T. Liang, X. Zeng, Z. Wen, L. Ren, R. Sun and X. Zeng, *ACS Appl. Polym. Mater.*, 2022, **4**, 4653–4663.
18 Y. S. Ju, *iScience*, 2022, **25**, 104587.
19 J. Wang, F. Ma and M. Sun, *RSC Adv.*, 2017, **7**, 16801–16822.
20 M. Jang, S. Singh and J. Suh, *Ceramist*, 2023, **26**, 106–120.
21 Y. Tao, S. Cai, C. Wu, Z. Wei, X. Lu, Y. Zhang and Y. Chen, *Phys. Lett. A*, 2022, **427**, 127920.
22 M. Li, B. Yin, C. Gao, J. Guo, C. Zhao, C. Jia and X. Guo, *Exploration*, 2023, **3**, 20210233.
23 Y. Ju Kwon, Y. Kim, Y.-P. Jeon, J.-Y. Hong, H. Seok Park and J. Uk Lee, *Composites, Part A*, 2022, **152**, 106675.
24 H. Li, W. Zheng, W. Liu and Q. Zhu, *Int. J. Heat Mass Transfer*, 2022, **196**, 123307.
25 T. Zhang, H. Wang, Y. Hao, J. Zhang, X. Sun and Y. Zeng, *Chin. J. Mater. Res.*, 2023, **37**, 401–407.
26 L. Li, *J. Compos. Sci.*, 2021, **5**, 187.
27 Y.-M. Jen, Y.-J. Chen and T.-H. Yu, *Polymers*, 2024, **16**, 3589.
28 J. M. Parente, P. Santos, S. Valvez, M. P. Silva and P. N. B. Reis, *Procedia Struct. Integr.*, 2020, **25**, 282–293.